Nanoporous Molecular Sandwiches: Pillared Two-Dimensional Hydrogen-Bonded Networks with Adjustable Porosity

Victoria A. Russell, Cara C. Evans, Wenjie Li, Michael D. Ward*

Crystal engineering of molecular materials is commonly frustrated by the absence of reliable structural paradigms that are needed for systematic design of crystal lattices with predictable structure and desirable function. This problem can be attributed, at least partially, to the absence of robust supramolecular motifs that serve as synthons for the assembly of crystal lattices. A novel class of molecular crystals based on two-dimensional hydrogen (H)-bonded networks comprising guanidinium ions and the sulfonate groups of alkane- or arenedisulfonate ions is described. The disulfonate ions act as pillars that connect opposing H-bonded sheets and form nanoporous galleries with one-dimensional channels. The flexibility of the H-bonded network allows the galleries to adapt to changes in the steric requirements of guest molecules that occupy the channels. This robustness reduces crystal engineering to the last remaining dimension, enabling rational adjustment of the gallery heights by choice of the disulfonate pillar.

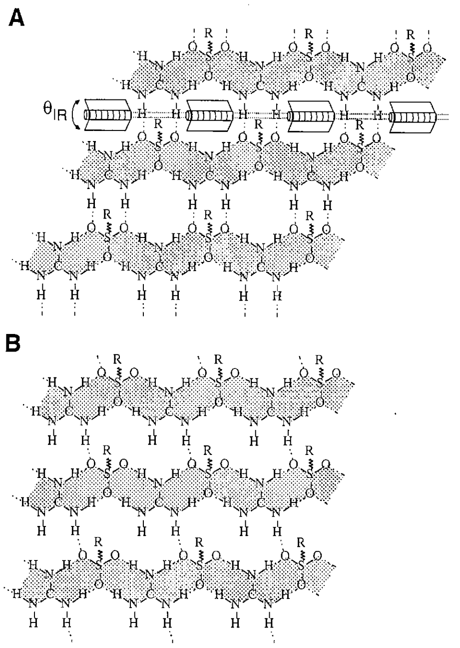

Fig. 1. Schematic representation of the sheetlike H-bonded networks formed from **G** cations and alkane- and arene-substituted monosulfonates and disulfonates. (**A**) The most commonly observed network is quasihexagonal, in which every sulfonate O atom is H-bonded to two **G** protons ($d_{O \cdot\cdot H} \approx 2.0$ Å) so that all H-bonding capacity is fulfilled. These sheets can be considered as assembling from 1D H-bonded ribbons (shaded) through H bonds. The interribbon puckering angle is described by θ_{IR}. (**B**) The shifted ribbon motif, in which adjacent ribbons are held together by one strong H bond ($d_{O \cdot\cdot H} \approx 2.0$ Å) and one weak H bond ($d_{O \cdot\cdot H} \approx 2.5$ Å) per **GS** pair, is observed in a minority of structures.

Interest in functional materials based on molecular crystals persists, owing to the potential for manipulating solid-state properties by systematic variations of the molecular structure and properties of the molecular components, a principal goal of crystal engineering (1). Recently, there has been growing interest in "nanoporous" molecular crystals, which in principle can provide molecular-scale voids with controlled sizes, shapes, and chemical environments that may be exploited for separations, shape-selective catalysis, and optoelectronic applications. Although there have been several examples of nanoporous lattices, which typically behave as hosts for molecular guests (2), systems amenable to controlled changes in void characteristics have been limited (3). In many cases, the formation of voids is somewhat serendipitous, as crystal engineering is commonly frustrated by an inability to predict solid-state structure precisely. A reasonable strategy for surmounting this obstacle is to use robust supramolecular "modules" (4) or "synthons" (5), for which "robust" is defined as the ability of the module to maintain its dimensionality and general structural features when changes occur in ancillary functional groups or other molecular species in the lattice. Robust n-dimensional modules can reduce the crystal engineering problem to 3-n dimensions, thereby simplifying materials design.

We recently reported molecular layered materials based on a two-dimensional (2D) H-bonded network composed of guanidinium cations (G) and the sulfonate groups of alkane- and arene-substituted monosulfonate anions (S) (6). The topological equivalence of the guanidinium ions and sulfonate groups, and strong (G)N–H···O(S) H bonds, favored the formation of quasihexagonal 2D **GS** networks in more than 30 different crystalline phases containing various sulfonate functionalities (Fig. 1A). The networks assembled in the third dimension as densely packed bilayers or as continuous stacks of interdigitated single layers due to van der Waals interactions between sulfonate R groups extending from the **GS** sheets (Fig. 2A). The pervasiveness of the **GS** sheets was attributed to their ability to form "accordion" or "pleated" sheets by puckering about (G)N–H···O(S) H-bonding "hinges" joining adjacent 1D ribbons. This puckering, which can be defined by interribbon dihedral angles of $\theta_{IR} < 180°$, enables the sheets to adapt to the steric demands of different R groups. In a few cases, these steric demands apparently were accommodated further by the formation of a shifted ribbon motif (Fig. 1B). Although considered to be less preferred than the quasihexagonal motif because of the loss of one strong H bond, 2D sheet formation in the shifted motif is enforced by the one remaining strong interribbon H bond.

The distinctive structural features of the **GS** networks prompted us to synthesize related materials in which the monosulfonate components were replaced with disulfonates. We anticipated that this would afford pillared bilayer structures, reminiscent of pillared metal organodiphosphonates (7). This substitution would result in a twofold reduction in alkyl group density, leading to the formation of voids in 2D galleries with sizes, heights, shapes, and chemical environments that could be manipulated by the choice of molecular pillar (Fig. 2B). The layering motif would depend on the sizes of the pillar and guest molecules that may occupy these voids. Sterically undemanding pillars and small guests would favor a bilayer motif, whereas large guests would favor a continuous single-layer stacking motif. Large pillars would favor only single-layer motifs with small guests or might even exclude guest molecules. The likelihood of these structures can be deduced from a simple geometric model that compares the area of a guest molecule, as projected onto the **GS** sheet, with the area available between the pillars in the different layering motifs (8).

We implemented this design strategy for the molecular pillars **I** to **VI**, which are depicted in Scheme 1 (**I** = dithionate; **II** = ethane-1,2-disulfonate; **III** = butane-1,4-disulfonate; **IV** = napthalene-2,6-disulfonate; **V** = biphenyl-4,4′-disulfonate; and **VI** = naphthalene-1,5-disulfonate). Crystalline forms of these materials can readily be obtained from methanol solutions by

---

Department of Chemical Engineering and Materials Science, University of Minnesota, Amundson Hall, 421 Washington Avenue SE, Minneapolis, MN 55455, USA.

*To whom correspondence should be addressed.

standard crystallization methods, and in most cases crystallization occurs rapidly upon standing in the growth solutions. Pillars **I** to **III** form bilayer galleries in which planar **GS** sheets ($\theta_{IR} = 180°$) are separated by the disulfonate pillars, which define 1D channels in the galleries (Fig. 3 and Table 1). The channel width is established by the distance between sulfur atoms within a given **GS** sheet ($d_{SS} \approx 7.5$ Å), and the height of the channel is established by the length of the pillar. Pillar **I** is exceptional because its C_{3V} symmetry enables $(\mathbf{G})_2\mathbf{I}$ to crystallize in the hexagonal space group $P6_3mc$, whereas the lower molecular symmetry of **II** and **III** forces a reduction of the lattice symmetry. The gallery thickness increases in the expected order $(\mathbf{G})_2\mathbf{I} < (\mathbf{G})_2\mathbf{II} < (\mathbf{G})_2\mathbf{III}$. The pillared regions of $(\mathbf{G})_2\mathbf{I}$ and $(\mathbf{G})_2\mathbf{II}$ are devoid of guest or solvent molecules, but the greater void height in $(\mathbf{G})_2\mathbf{III}$ accommodates two acetonitrile (CH_3CN) guest molecules in the lattice. The butyl residues exhibit the less favorable gauche conformation, apparently to optimize packing of the guest in the pillared layers. Upon standing in air, the CH_3CN guests in $(\mathbf{G})_2\mathbf{III} \cdot 2CH_3CN$ rapidly escape the host lattice to afford a nonlayered guest-free phase in which the butyl chains adopt the more favorable anti conformation (*9*). The absence of a guest-free $(\mathbf{G})_2\mathbf{III}$ bilayer structure most likely is due to its low packing fraction (PF) of 0.55, as calculated after computer removal of the guest from $(\mathbf{G})_2\mathbf{III} \cdot 2CH_3CN$ (*10*). The PF of $(\mathbf{G})_2\mathbf{II}$ (0.59) is intermediate between this value and that of $(\mathbf{G})_2\mathbf{III} \cdot 2CH_3CN$ (0.68); organic crystals typically exhibit a PF > 0.65. This suggests that the PF of $(\mathbf{G})_2\mathbf{II}$ is near the lower stability limit for guest-free pillared **GS** bilayers. Propane-1,3-disulfonate forms only a nonlayered phase, free of guests, that can be attributed to the conformational constraints of this pillar and excessive void space (*11*).

We anticipated that increased conformational rigidity in pillars **IV** to **VI** would impart even greater stability to bilayer galleries. In the case of $(\mathbf{G})_2\mathbf{IV} \cdot$ benzonitrile, which crystallizes from methanol solutions containing benzonitrile, the naphthyl residues in the gallery form the walls of 1D channels oriented along a H-bonded ribbon direction of the quasihexagonal **GS** sheet. As expected from the axial length of **IV**, the gallery height is greater than that achieved with pillars **I** to **III**. This enables inclusion of the larger benzonitrile guest molecules, which form 1D arrays parallel to the channel direction (Fig. 4A).

The pillared bilayer structure is also observed for $(\mathbf{G})_2\mathbf{V} \cdot 2MeOH$ (MeOH, methanol) upon crystallization from MeOH solutions. However, the gallery height is substantially less than expected, owing to severe tilting of the pillars. The pillars define 1D channels parallel to one of the H-bonded ribbons of the quasihexagonal **GS** sheet, with the pillars alternating orientation along the channel (the angle subtended by the long axes of adjacent biphenyl residues, as viewed along the channel, is 63°). These channels are occupied by MeOH guests organized as 1D H-bonded chains along the channel axis. The pillar tilting results in an atypical corrugation of the 2D **GS** sheet in which the sulfonate head groups are tilted substantially out of the **GS** sheet. Nevertheless, the quasihexagonal topology is retained with normal (G)N–H · · · O(S) H-bonding distances, demonstrating the flexibility of the 2D network.

The presence of guests, such as *m*-xylene (*m*-xyl), styrene (sty), and toluene (tol), in the MeOH crystallization solutions results in the formation of crystalline phases $(\mathbf{G})_2\mathbf{V} \cdot Ar$ (Ar, arene) in which the Ar guests are incorporated instead of MeOH. The greater size of these guests results in a reduction in the tilting of the biphenyldisulfonate pillars, which form densely packed walls of 1D channels occupied by the guests (Fig. 4A). Unlike the aforementioned phases, the **GS** sheets exhibit the shifted ribbon motif, and the channels are oriented per-

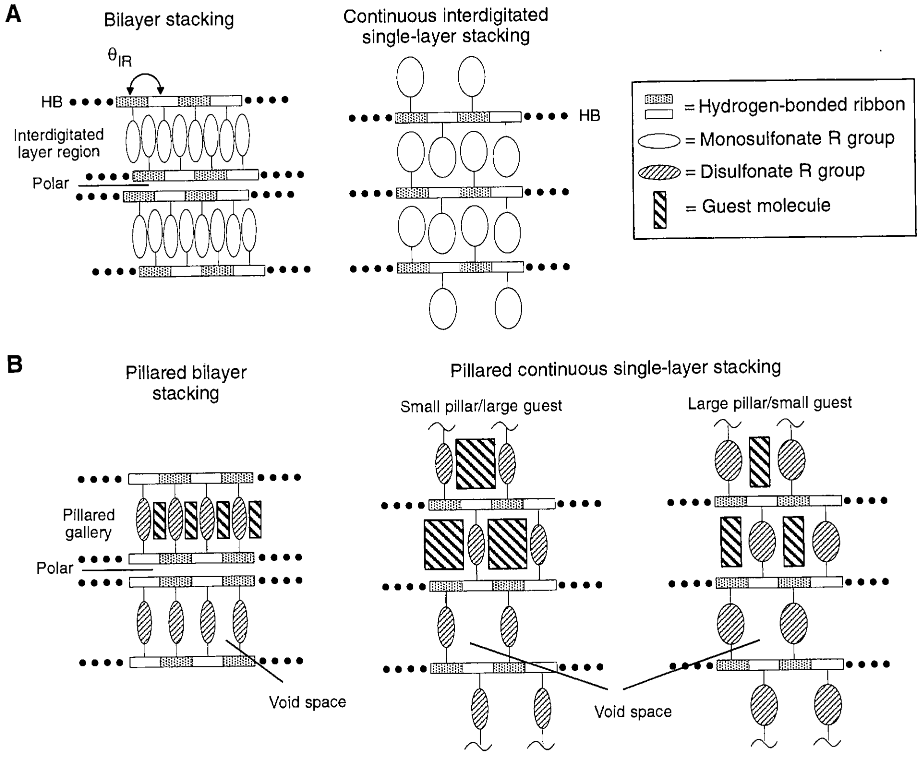

Fig. 2. Schematic representations of layered materials synthesized from **G** cations and alkane- and arene-substituted monosulfonates and disulfonates, as viewed along the long axis of the H-bonded ribbons contained in the nominally planar **GS** networks. The white and shaded rectangles represent the narrow edges of the ribbons. (**A**) Two stacking arrangements of the nominally planar **GS** networks observed for **G** monosulfonates. Bilayer motifs are observed for R groups that are small enough to allow interdigitation in the nonpolar region separating the **GS** sheets. If the alkyl or aryl groups are too large, the R groups of adjacent ribbons are oriented to opposite sides of each sheet, which provides room for interdigitation and the continuous single-layer stacking of the **GS** sheets. The sheets can adapt further to the steric requirements of the R groups in either layering motif by puckering about (**G**)N–H · · · O(**S**) H-bonding "hinges" between adjacent ribbons (θ_{IR}). (**B**) Analogous possible layering motifs for **G** disulfonates. The twofold reduction in the number of alkyl groups in the pillared region opens nanoscale voids capable of enclathrating molecular guests. The layering motif is governed by the combined size of pillar and guest.

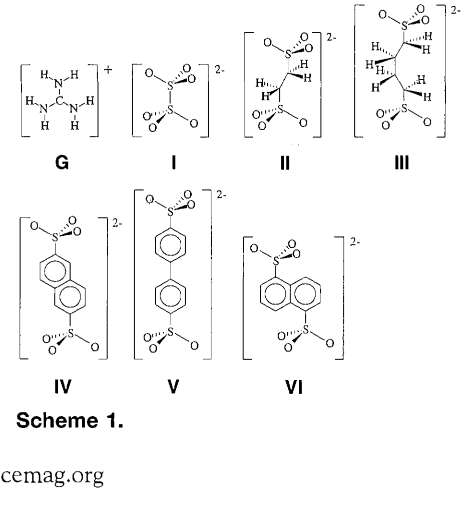

Scheme 1.

Table 1. Summary of structural features of pillared **GS** H-bonding networks.

Compound	Space group	Lattice parameters *a* (Å) (α)	 *b* (Å) (β)	 *c* (Å) (γ)	Gallery height (Å)	θ_{IR} (degrees)	PF (with guest)	PF (without guest)
(G)$_2$**I**	*P*6$_3$*mc*	7.504	7.504	12.129	3.0	180	*	0.67
(G)$_2$**II**	*C*2/*m*	12.80	7.34 (96.1°)	8.46	5.5	180	*	0.59
(G)$_2$**III** · 2CH$_3$CN	*C*2/*c*	22.860	7.260 (106.63°)	12.876	8.3	180	0.68	0.55
(G)$_2$**IV** · benzonitrile	*P*$\bar{1}$	7.270 (83.344°)	7.410 (88.186°)	12.694 (61.872°)	9.51	180	0.70	0.53
(G)$_2$**V** · 2MeOH†	*P*2$_1$/*c*	12.010	27.035 (92.437°)	7.432	8.9	180	0.67	0.55
(G)$_2$**V** · *m*-xyl‡	*P*$\bar{1}$	7.251 (78.781°)	12.328 (84.872°)	29.376 (86.372°)	11.5	180	0.69	0.52
(G)$_2$**V** · tol‡	*P*$\bar{1}$	6.166 (96.898°)	7.307 (93.068°)	14.076 (92.397°)	11.1	180	0.68	0.53
(G)$_2$**V** · sty‡	*P*$\bar{1}$	6.170 (96.304°)	7.268 (92.817°)	14.086 (93.253°)	11.1	180	0.70	0.53.53
(G)$_2$**VI** · 2MeOH	*Pbam*	7.891	18.718	7.408	-	42	0.54	0.47
(G)$_2$**VI** · 2propanenitrile	*Pbam*	7.884	19.221	7.423	-	41	0.60	0.46
(G)$_2$**VI** · 1-hexanenitrile	*Pnnm*	7.721	21.437	7.468	-	61	0.60	0.42
(G)$_2$**VI** · 1-octanenitrile	*Pnnm*	8.935	19.837	7.632	-	89	0.66	0.46
(G)$_2$**VI** · 1,6-hexanedinitrile	*Cmc*2$_1$	7.445	40.892	8.096	-	74	0.60	0.43
(G)$_2$**VI** · triglyme	*Pbam*	7.848	19.035	7.449	-	34	0.71§; 0.65‖	0.56

*No guest included in lattice. †The tilt of the sulfonate head group out of the **GS** sheet plane is 146°. The **G** ions are all contained within the same plane, so θ_{IR}, as defined by Fig. 1, actually is $\theta_{IR} = 180°$. ‡The angles of pillar tilt parallel and perpendicular to the channel direction, respectively, are 10° and 8° for **(G)**$_2$**IV** · xyl, 19° and 6° for **(G)**$_2$**IV** · tol, and 19° and 8° for **(G)**$_2$**IV** · sty. §Based on an occupancy of one triglyme per two units of host, as suggested by nuclear magnetic resonance. ‖Based on an occupancy of 2/3 triglyme per two units of host, as suggested by x-ray diffraction. The triglyme guest was severely disordered, which complicates precise determination of the occupancy by x-ray diffraction.

pendicular to the H-bonded ribbons. The average PF of the guest-free phases, calculated after computer removal of the guest molecules, is approximately 0.52. This value increases to roughly 0.69 when guests are included in the calculations. The retention of the pillared bilayer structure for the differently sized MeOH and Ar guests illustrates the adaptiveness of the GS networks, which enables space-filling to be optimized in the gallery regions. This adaptiveness also is evident from specific structural features of the (G)$_2$V phases. The pillar tilt is smaller and the gallery height larger for (G)$_2$V · *m*-xyl than for (G)$_2$V · tol and (G)$_2$V · sty. This is due to the increased steric demand along the gallery height imposed by the *m*-xyl methyl groups, which project vertically toward opposite GS sheets of the bilayer. Furthermore, the dihedral angle subtended by the phenyl rings within each biphenyl pillar is 25° for (G)$_2$V · *m*-xyl and 31.5° for (G)$_2$V · 2MeOH, but 0.6° for (G)$_2$V · tol and (G)$_2$V · sty. The twisting of the biphenyl pillars in the former pair reflects the tendency to reduce *ortho*-hydrogen steric interactions (*12*), which is made possible by the void space created in the vertically expanded galleries in (G)$_2$V · *m*-xyl and the small guests in (G)$_2$V · 2MeOH. The planar biphenyl structure in the other two phases indicates that the *ortho*-hydrogen steric interactions are compensated by packing forces between planar biphenyl pillars and Ar guests, in the gal-

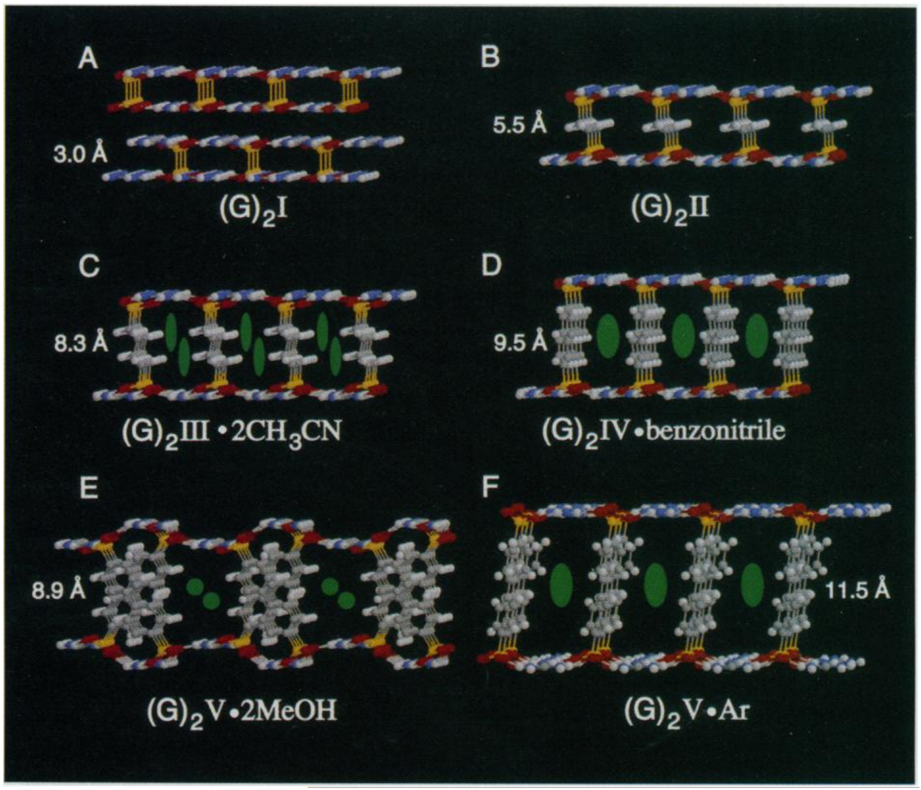

Fig. 3. (**A** through **F**) Pillared bilayer motifs, as determined by single-crystal x-ray diffraction, in **G** salts of the alkane- and arenedisulfonates depicted in Scheme 1. The views are rotated slightly to depict the walls of the 1D channels in the galleries. In all cases, the bilayers stack in the solid state as illustrated for **(G)**$_2$**I** in (A). The guest molecules occupying the nanoporous voids in the galleries are depicted as green circles or ovals for clarity. The gallery heights, as measured by the distance between the **G** ion mean planes of opposing **GS** sheets, are indicated. The gallery height depicted in (F) is for **(G)**$_2$**IV** · *m*-xyl. Atom identification: C, gray; H, white; N, blue; O, red; and S, yellow.

leries of reduced height. The influence of packing forces on the conformation of crystalline biphenyl and related derivatives has been described previously (*13*).

Contrary to the aforementioned examples, the napthalene-1,5-disulfonate pillar **VI** forms pillared phases in which severely puckered quasihexagonal **GS** sheets assemble in the third dimension by continuous single-layer stacking. For example, (G)$_2$**VI** · 2MeOH crystallizes from MeOH solutions as an orthorhombic phase with 1D channels oriented perpendicular to the H-bonded ribbon direction and occupied by MeOH guests. The channel walls consist of naphthalene pillars whose molecular planes are parallel to the channel direction (Fig. 4B). The channel widths are established by the nominal distance between sulfur atoms in the quasihexagonal sheet (d_{SS} = 7.5 Å). Crystallization of (G)$_2$**VI** phases from MeOH solutions containing linear substituted alkanes such as 1-alkanenitriles, α,ω-alkanedinitriles, 1-alkanols, and triglyme afford the same orthorhombic host lattice but with these molecules occupying the channels instead of MeOH. The (G)$_2$**VI** lattice was highly selective for 1-alkanenitriles, with incorporation of $CH_3(CH_2)_5CN$ and $CH_3(CH_2)_4CN$ highly preferred among this class of guests (*14*). The guest molecules typically were disordered, but the structure of the host lattice was determined easily in all cases. Although the topology of the (G)$_2$**VI** host lattices is independent of the identity of the guest, θ_{IR} ranges from 34° to 89°. Because the channels are oriented perpendicular to the H-bonded ribbons, decreasing θ_{IR} values [increasing puckering about the interribbon (G)N–H···O(S) H bonds] correspond to decreasing channel lattice constants. This suggests that the 1D channels can adapt to different guest lengths by network puckering, possibly driven by commensurism between the host and guest sublattices. The packing fractions of the phases occupied by guests are rather low, reflecting the robustness of these networks. We note that the guest molecules can be driven from the host lattice by heating above 180°C to yield a new crystalline phase, for which a structure has not been determined.

Molecular modeling indicates that a pillared bilayer structure with **VI** is feasible. The sterically optimum bilayer structure contains isolated voids in the gallery that are not large enough to incorporate even small guests such as MeOH (modeling reveals that the formation of continuous 1D channels in the gallery, which would be capable of incorporating linear guests, is prohibited by steric interactions between the pillars in this configuration). The absence of this apparently reasonable bilayer structure suggests that crystallization of the (G)$_2$**VI** salts is driven by template-directed assembly in which the host preferentially organizes about the linear guests (or MeOH) to produce the observed densely packed 1D channels. This resembles templating mechanisms proposed for the formation of zeolite and inorganic networks around molecular species (*15*).

The synthesis of these nanoporous networks demonstrates that solid-state motifs can be predictable if modules are used that can maintain their structural dimensionality and integrity with changes in ancillary functional groups. The use of the robust 2D **GS** networks reduces the crystal engineering problem to the last remaining dimension, so that the pillar structure and nanopore dimensions can be adjusted rationally. The robustness of the **GS** networks can be attributed to their ability to adapt to the steric demands of different guest molecules without loss of the 2D architecture. The **GS** networks adapt by (i) puckering of the **GS** sheet about interribbon (G)N–H···O(S) H-bonded "hinges," (ii) switching between the quasihexagonal and shifted ribbon motifs, (iii) tilting of the pillars so that the network can shrink around the guest molecules, which is made possible by the flexibility of the (G)N–H···O(S) H bonds, and (iv) adjusting the conformations of the pillars to optimize packing in the galleries. It also is important to note that the use of dense 2D H-bonded networks such as the **GS** sheets prevents the network interpenetration that commonly frustrates the formation of voids in molecular crystals. These networks provide a platform for fundamental studies of solid-state structure, and we

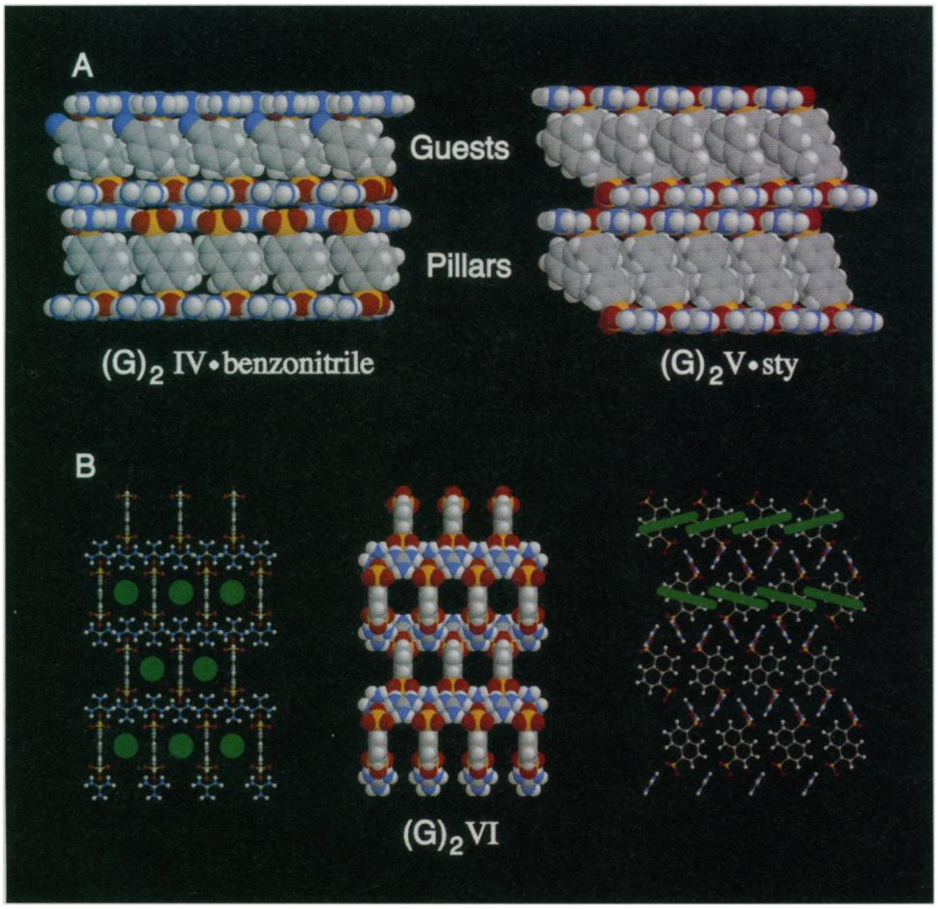

Fig. 4. (**A**)(**G**)$_2$**IV** · benzonitrile and (**G**)$_2$**V** · sty as viewed perpendicular to the channel directions. Each model is depicted so that the top channel reveals the guest molecules in front of the pillars and the bottom channel illustrates the pillars in front of the guests. (**B**) The pillared, continuous, single-layer stacking motif in (**G**)$_2$**VI**, as viewed along the 1D channels in ball-and-stick (left, with green circles signifying linear-substituted alkane guest molecules) and space-filling formats (center, with guests omitted for clarity). The H-bonded ribbons run horizontally in the plane of the page. The right panel is a cutaway view illustrating the channel structure as viewed perpendicular to the channel, revealing the highly puckered nature of the pleated **GS** sheet. The H-bonded ribbons are perpendicular to the channel direction, and therefore project out from the plane of the paper. Guest molecules are depicted generically as green rods in the upper two channels. Atom identification: C, gray; H, white; N, blue; O, red; and S, yellow.

anticipate that analogs in which the disulfonate pillars have specific functionality will have potential as host lattices for optoelectronic materials, molecular separations, and chemical reactions performed in the nanoscale voids.

REFERENCES AND NOTES

1. G. M. J. Schmidt, *Pure Appl. Chem.* **27**, 647 (1971); G. R. Desiraju, *Crystal Engineering: The Design of Organic Solids* (Elsevier, New York, 1989).
2. *Comprehensive Supramolecular Chemistry*, J. L. Atwood, J. E. D. Davies, D. D. MacNicol, F. Vogtle, Eds. (Pergamon, New York, 1996), vol. 6; V. Ramamurthy and D. F. Eaton, *Chem. Mater.* **6**, 1128 (1994); J. Wang, M. Simard, J. D. Wuest, *J. Am. Chem. Soc.* **116**, 12119 (1994); G. B. Gardner, D. Venkataraman, J. S. Moore, S. Lee, *Nature* **374**, 792 (1995); B. F. Hoskins and R. Robson, *J. Am. Chem. Soc.* **112**, 1546 (1990); D. M. L. Goodgame, S. Menzer, A. M. Smith, D. J. Williams, *Angew. Chem. Int. Ed. Engl.* **34**, 574 (1995); J. Hulliger, O. Konig, R. Hoss, *Adv. Mater.* **7**, 719 (1995); P. R. Ashton *et al.*, *Angew. Chem. Int. Ed. Engl.* **34**, 1862 (1995); S. V. Kolotuchin, E. E. Fenlon, S. R. Wilson, C. J. Loweth, S. C. Zimmerman, *ibid.*, p. 2654; M. D. Hollingsworth, M. E. Brown, A. C. Hillier, B. D. Santarsiero, J. D. Chaney, *Science* **273**, 1355 (1996); D. Venkataraman, S. Lee, J. Zhang, J. S. Moore, *Nature* **371**, 591 (1994).
3. O. Ermer, *J. Am. Chem. Soc.* **110**, 3747 (1988); ______ and L. Lindenberg, *Helv. Chim. Acta* **74**, 825 (1991).
4. V. A. Russell and M. D. Ward, *Chem. Mater.* **8**, 1654 (1996).
5. G. R. Desiraju, *Angew. Chem. Int. Ed. Eng.* **34**, 2311 (1995).
6. V. A. Russell, M. C. Etter, M. D. Ward, *J. Am. Chem. Soc.* **116**, 1941 (1994); *Chem. Mater.* **6**, 1206 (1994); V. A. Russell and M. D. Ward, *Acta Crystallogr.* **B52**, 209 (1996).
7. Y. P. Zhang and A. Clearfield, *Inorg. Chem.* **31**, 2821 (1992); G. Cao, H.-G. Hong, T. E. Mallouk, *Acc. Chem. Res.* **25**, 420 (1992); M. E. Thompson, *Chem. Mater.* **6**, 1168 (1994); K. P. Reis, V. K. Joshi, M. E. Thompson, *J. Catal.* **161**, 62 (1996); G. Cao and T. E. Mallouk, *J. Solid State Chem.* **94**, 59 (1991).
8. A simple model based on a 2D planar **GS** sheet and idealized cylindrical guests indicates that the diameter of the guest molecule (D_g) must be $D_g < 2\sqrt{3} \cdot d_{SS} - D_p$ for the bilayer motif and $D_g < 2 \cdot d_{SS} - D_p$ for the continuous single-layer stacking motif, where d_{SS} is the distance between nearest neighbor sulfur atoms in a **GS** sheet (approximately 7.5 Å), and D_p is the diameter of the pillar as projected onto the **GS** sheet. If the guest is a flat monolith oriented along the channel direction, the width of the guest (W_g), as projected onto the **GS** sheet, must be $W_g < \sqrt{3/2} \cdot d_{SS} - D_p$ for the bilayer motif and $W_g < \sqrt{3} \cdot d_{SS} - D_p$ for the continuous single-layer stacking motif.
9. This nonlayered guest-free phase of $(\mathbf{G})_2\mathbf{III}$ also can be crystallized directly from water in the absence of acetonitrile: space group $P2_1/n$, a = 7.958 Å, b = 10.936 Å, c = 8.346 Å, β = 92.070°. This phase is identical to that obtained by removal of CH_3CN guests from $(\mathbf{G})_2\mathbf{III} \cdot 2CH_3CN$.
10. Packing fraction values were calculated from Connolly surfaces using Cerius^2 molecular modeling software (version 1.6). A comparison of arbitrarily chosen examples from the Cambridge Structural Database revealed that the PF values calculated with Cerius^2 are systematically lower, by an average of 1.2%, than Ck values reported by others [see A. I. Kitaigorodskii, *Molecular Crystals and Molecules* (Academic Press, New York, 1973), and A. Gavezzotti, *Nouv. J. Chim.* **6**, 443 (1982)].
11. A nonlayered guest-free phase $(\mathbf{G})_2$(propane-1,3-disulfonate) can be crystallized from water. Molecular models indicate that the voids in a propane-1,3-disulfonate bilayer structure would not be large enough to accommodate molecular guests that would be needed to stabilize the lattice. Furthermore, a bilayer structure would require an unfavorable eclipsed conformation along one of the carbon-carbon bonds of this pillar.
12. The twist angles for biphenyl in the solution and gas phases lie in the ranges 20° to 25° and 40° to 45°, respectively [see O. Bastiansen and S. Samdal, *J. Mol. Struct.* **128**, 115 (1985), and G. Casalone, C. Mariani, A. Mugnoli, M. Simonetta, *Mol. Phys.* **15**, 339 (1968)].
13. The twist angle in crystalline biphenyl is 0°, whereas the twist angles in crystalline substituted biphenyls range from 0° to 47.2° [see G.-P. Charbonneau and Y. Delugeard, *Acta Crystallogr.* **B33**, 1586 (1977), and C. P. Brock and R. P. Minton, *J. Am. Chem. Soc.* **111**, 4586 (1989)].
14. The selectivity profiles for 1-alkanenitriles $CH_3(CH_2)_n$-CN, using $n = 5$ as a basis, were determined to be 0.13 ($n = 6$), 1.0 ($n = .5$), 0.67 ($n = 4$), 0.04 ($n = 3$), 0.01 ($n = 2$), and 0.01 ($n = 1$). The selectivity trends for 1-alkanols $CH_3(CH_2)_nCH_2OH$, using $n = 5$ as a basis, were similar, with 1.1 ($n = 6$), 1.0 ($n = 5$), 0.71 ($n = 4$), 0.23 ($n = 3$), 0.48 ($n = 2$), and 0.20 ($n = 1$). The selectivity ratios for 1-alkanenitrile inclusion over 1-alkanol inclusion for equivalent n were 3.0 ($n = 6$), 6.3 ($n = 5$), 10.0 ($n = 4$), and 1.4 ($n = 3$).
15. M. E. Davis, A. J. Katz, W. R. Ahmad, *Chem. Mater.* **8**, 1820 (1996).
16. We thank V. Young, D. Britton, and W. Ojala (University of Minnesota) for crystallographic services and NSF for financial support. Supplementary material, including crystallographic reports and coordinates, is available on request.

4 December 1996; accepted 7 February 1997

Scanning Single-Electron Transistor Microscopy: Imaging Individual Charges

M. J. Yoo,* T. A. Fulton, H. F. Hess, R. L. Willett, L. N. Dunkleberger, R. J. Chichester, L. N. Pfeiffer, K. W. West

A single-electron transistor scanning electrometer (SETSE)—a scanned probe microscope capable of mapping static electric fields and charges with 100-nanometer spatial resolution and a charge sensitivity of a small fraction of an electron—has been developed. The active sensing element of the SETSE, a single-electron transistor fabricated at the end of a sharp glass tip, is scanned in close proximity across the sample surface. Images of the surface electric fields of a $GaAs/Al_xGa_{1-x}As$ heterostructure sample show individual photo-ionized charge sites and fluctuations in the dopant and surface-charge distribution on a length scale of 100 nanometers. The SETSE has been used to image and measure depleted regions, local capacitance, band bending, and contact potentials at submicrometer length scales on the surface of this semiconductor sample.

Inspired by the development of the scanning tunneling microscope, a variety of surface scanning probes (*1*) have been developed to measure and map properties of material surfaces on a microscopic scale. In particular, surface electrical properties have been explored with noncontact techniques such as scanning capacitance microscopy (*2*), scanning Kelvin probe microscopy (*3*), and electric-field–sensitive atomic force microscopy (EFM) (*4*). Indeed, the last has in one instance (*5*) shown the remarkable ability to detect the presence of individual charges and to obtain images of insulating surfaces in which a charged spot of one or two electrons is apparent.

We report the development of a low-temperature scanning electrometer operating on a different principle, one which has one to two orders of magnitude greater charge resolution and a similar spatial resolution (100 nm) compared with the EFM. This microscope, the single-electron transistor (SET) scanning electrometer, or SETSE, uses the SET as a probe to sense the electrically induced charge on its small (100 nm) metal island held in proximity to the sample surface (Fig. 1C). It can detect ~1% of an electron charge (0.01e). Because all of the important geometrical parameters are known, one can assign a quantitative interpretation to the SETSE signal. Also, during operation the SETSE, unlike the EFM, does not require the application of high electric fields (10^6 V cm^{-1}) between the tip and surface, an important consideration for many interesting but easily perturbed semiconductor systems. All of these features enable a broader class of experiments to be explored.

As an example, we studied the electric fields at the surface of a semiconductor $GaAs/Al_xGa_{1-x}As$ heterostructure sample. These fields arise from localized charges at and near the surface as well as from the voltage bias and work function of any underlying electrode. Statistical fluctuations in the density of surface charges are evident, although the individual charges are too closely spaced (<10 nm) to be resolved directly. However, we are able to image the more widely spaced individual charges that are produced by brief light exposure. These

---

Lucent Technologies, Bell Laboratories, Murray Hill, NJ 07974, USA.

*Present address: Philips Laboratories, 345 Scarborough Road, Briarcliff Manor, NY 10510, USA.